Review Article

Iron Oxide–Enhanced MR Imaging of the Liver and Spleen: Review of the First 5 Years

Joseph T. Ferrucci[1] and David D. Stark

American Journal of Roentgenology 1990;155:943-950.

Superparamagnetic iron oxide (SPIO) particles are a potent new class of MR contrast agents affording improved detection of hepatic and splenic neoplasms. In this report we review the development of this agent through preclinical studies and early clinical results at Massachusetts General Hospital during a 5-year investigation. SPIO particles are sequestered by normal phagocytic Kupffer cells of the reticuloendothelial system (RES) but are not retained in tumor tissue. Consequently, there is a fivefold increase in T2 relaxation between normal RES tissue and tumor, with a comparable advantage in quantitative signal-to-noise ratio, contrast-to-noise ratio, and lesion detectability in the liver and spleen on MR imaging. Increased lesion conspicuity can be exploited to decrease threshold size for lesion detection to less than 3 mm. Clinically beneficial effects occur with a variety of mildly T2-weighted spin-echo pulse sequences; gradient-echo techniques show even greater benefit after administration of SPIO. Metabolically, pharmaceutical-grade preparations are biodegradable and bioavailable, being rapidly turned over into body iron stores and incorporated into erythrocyte hemoglobin. Early dose-escalation clinical trials have identified a probable clinical dose range of 10–20 μmol Fe/kg body weight. In the United States, SPIO compounds evaluated to date are still approved for use in investigational studies only. Newer commercial formulations currently being evaluated may extend clinical safety margins.

Iron oxide, in the form of superparamagnetic particles, is a powerful tissue-specific MR contrast agent used for enhanced detection of tumors in the liver and spleen. Extensive preclinical studies at the Massachusetts General Hospital from 1985 through 1988 elucidated the biological and pharmaceutical principles for MR imaging [1–7] and led to the first clinical trial in 1988, in which greatly enhanced detection of liver lesions was confirmed [8]. Additional clinical trials are now in progress in the United States as well as in France, Belgium, and Japan, and early results from one European center recently have been reported [9]. The potential benefits of superparamagnetic iron oxide (SPIO) particles have been widely recognized by the MR contrast media research community, but, in the United States, these agents are still approved for use only in investigational studies.

This article reviews the development of iron oxide–enhanced MR imaging of the liver and spleen during the past 5 years. The emphasis is on work carried out by the Division of Gastro-Intestinal Radiology at the Massachusetts General Hospital.

Superparamagnetic Iron Oxide: Physical Properties

SPIO particles are crystalline structures with the general formula $Fe^{3+}{}_2O_3M^{2+}O$, where M^{2+} is a divalent metal ion like iron, manganese, nickel, cobalt, or magnesium. SPIO is similar to magnetite, a naturally occurring ferrite, in which the metal ion (M^{2+}) is ferrous iron (Fe^{2+}) with the formula Fe_3O_4 (Fig. 1).

Received May 11, 1990; accepted after revision June 14, 1990.
Presented at the International Symposium on Liver Imaging, Harvard Medical School, Boston, June 1990.
[1] Both authors: Department of Radiology, Massachusetts General Hospital and Harvard Medical School, 55 Fruit St., Boston, MA 02115. Address reprint requests to J.T. Ferrucci.

American Journal of Roentgenology 1990;155:943-950.

Because of its ubiquitous presence in living tissue, iron is a natural candidate for manipulation of MR signal. Indeed, the ferrite magnetite is particularly suitable because this iron oxide has been isolated from certain birds, fish, and bacteria in which its interaction with the magnetic field of the earth has been found to play a critical role in navigation [10].

Pharmaceutical-grade preparations suitable for clinical use have evolved rapidly since the earliest characterization studies of magnetic particles for possible medical applications were performed [1–3]. Superparamagnetic iron oxide crystals by themselves are 5–50 nm in size. However, these crystals are usually formed by precipitation of iron salts with coating material to form larger composite particles. The median diameter of composite particle size has been varied from the 1000-nm range used in early studies to less than 10 nm (Fig. 2). The smaller size of newer particles accelerates degradation of SPIO into paramagnetic forms of iron. Biocompatible coatings such as starch (dextran), protein, glycoprotein, or lipid allow safe IV administration and ready biodegradability. The compound used in our initial clinical trials was a stable colloidal aqueous suspension of iron oxide–dextran, reddish brown to black, formulated at 0.2 mmol/l Fe and designated AMI-25 or Feridex (Advanced Magnetics, Inc., Cambridge, MA).

The magnetic properties of these materials were first referred to as superparamagnetic in 1955 [11]. The term refers to the extremely large magnetic moments they acquire when placed in external magnetic fields. This sensitivity to magnetic fields is the result of the crystalline matrix, which facilitates the alignment of adjoining spins to an applied field. This is so efficient that even at low field strengths all available spins can be recruited, and no further gain in magnetization is achieved by increasing the applied field strength. Superparamagnetic materials differ from ferromagnetic substances because, like diamagnetic and paramagnetic materials, they do not retain any magnetization once the external field is removed. In contrast, once magnetized, ferromagnetic materials show remanence (i.e., remain partially magnetized even in the absence of an applied field), and therefore are used as recording materials and to make permanent magnets.

In tissue, the large magnetic moments associated with superparamagnetic iron particles result in local magnetic field inhomogeneities. Diffusion of water through these local field disturbances produces rapid proton dephasing, which results in preferential shortening of transverse relaxation time, T2, with little effect on longitudinal relaxation time, T1. The T2 relaxivity (R2) of 1×10^5 sec^{-1} $(mol/l)^{-1}$ and T1 relaxivity (R1) of 3×10^4 sec^{-1} $(mol/l)^{-1}$ of iron oxide are substantially larger than the relaxation of paramagnetic molecules such as gadopentetate dimeglumine: R2 = 6×10^3 and R1 = 4×10^3 sec^{-1} (mol/l^{-1}) [1–7].

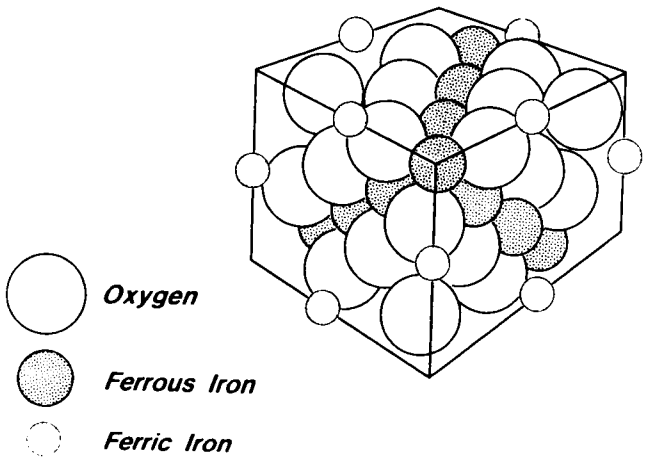

Fig. 1.—Drawing shows spinel crystal structure characteristic of superparamagnetic iron oxides.

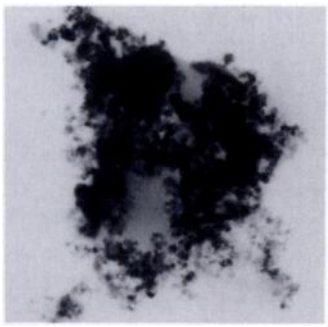

Fig. 2.—Electron micrograph of superparamagnetic iron oxide particle (M4125, Advanced Magnetics, Inc., Cambridge, MA) magnified ×82,000 shows an irregularly shaped structure approximately 1 μm in size. Particle shape and size are stabilized by coating a cluster of iron oxide crystals with a hydrophilic polymer. Individual superparamagnetic ferrite crystals can be seen. (Reprinted with permission from Saini et al. [1].)

Superparamagnetic Iron Oxide: Physiologic Considerations

Pharmacokinetic behavior of SPIO is generally comparable in animals and humans [1–7]. The injected particles are smaller than erythrocytes (which are approximately 7 μm in diameter), so they successfully traverse capillary beds in the lung, brain, heart, and kidney. Particles are promptly sequestered by the reticuloendothelial system (RES). The RES cells have a scavenging function and, by phagocytosis, readily remove particulate materials from the circulation. AMI-25 shows a blood clearance half-life of about 10 min with uptake by hepatic RES Kupffer cells accounting for 80% of the injected dose [1–7]. Thus, T2 relaxation times of blood, liver, and spleen decrease promptly after IV injection, but only blood quickly returns to normal. The extremely powerful effect that SPIO particles have on proton relaxation is attested to by the observation that even in minute doses (8 μmol/kg), which are located in a very small (approximately 2%) portion of the hepatic cellular volume (i.e., Kupffer cells), there is essentially complete signal loss from the entire liver.

Because neoplastic tumor nodules are devoid of the phagocytic Kupffer cells, they do not sequester SPIO (Fig. 3). As a consequence, the signal difference between normal RES tissue and tumor is greatly enhanced. After administration of SPIO, no change occurs in relaxation times of tumor, whereas normal liver shows an almost threefold decrease in T2. The resulting difference in T2 relaxation between tumor and liver, expressed as a percentage of T2 of normal liver, increased from 49% to 280% in ex vivo studies of a rat liver-tumor model [2].

To date, newer formulations of SPIO have been evaluated in animals only. Ferrosomes are a class of SPIO encapsulated

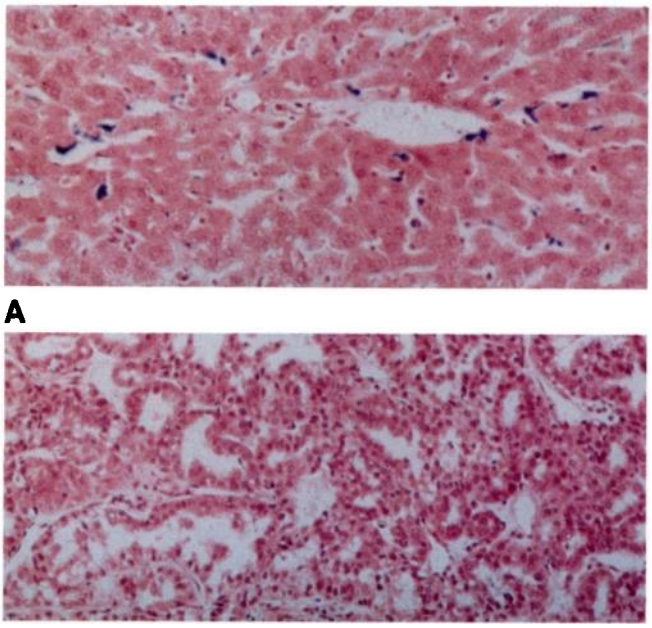

Fig. 3.—Reticuloendothelial sequestration of IV administered superparamagnetic iron oxide particles in normal liver but not in tumor tissue.

***A* and *B*, Light microscopic sections of normal rat liver (*A*, ×320) and tumor tissue (*B*, ×200) stained for iron (Prussian blue). Superparamagnetic iron oxide particles are stained blue and can be identified readily in hepatic reticuloendothelial cells. No such particles are present in hepatocytes or in tumor tissue. (Reprinted with permission from Saini et al. [2].)**

in lipid vesicles (liposomes) developed by Vestar, Inc. (San Dimas, CA) that have prolonged blood circulation (clearance half-life, 4 hr). Prolonged circulation allows increased delivery of SPIO to tissues other than the liver and spleen. For example, ferrosomes show distribution to macrophages located at the periphery of tumors [12].

Metabolically, AMI-25 iron is biodegradable and bioavailable, being rapidly turned over into the body iron stores and incorporated into erythrocytes as hemoglobin [6]. In studies that used light microscopy, stainable iron disappears from rat liver within 2 weeks, whereas radiolabeled ^{59}Fe iron oxide shows a liver-spleen half-life of 3–4 days [7]. With in vivo MR imaging in animals as well as humans, liver signal blackening shows a reversal toward normal baseline tissue characteristics over 3–7 days [1, 8].

Bioavailability is demonstrated by the incorporation of molecular iron into hemoglobin after administration of ^{59}Fe AMI-25. Twenty percent of radiolabeled iron is found in hemoglobin 14 days after IV administration. Similar rates of erythrocyte incorporation (21%) occur with administration of radiolabeled ferritin. Bioavailability is shown also by the ability of SPIO to reverse iron-deficiency anemia in rats to an extent similar to that of hematinic iron-dextran [6].

Extensive toxicity studies in animals have disclosed no acute toxic effects (LD_{50} in rats) or chronic injury at doses greater than 100 times the clinically effective dose of 20 μm Fe/kg body weight [3, 6]. Even at the subcellular level, when a massive dose of 250 mg Fe/kg was given to rats, Bacon et al. [3] were unable to detect hepatic mitochondrial dysfunction or microsomal lipid peroxidation, both sensitive biochemical indicators of iron-induced hepatotoxicity. Despite the large increase in hepatic iron concentrations at 10 weeks after SPIO administration, biochemical and morphologic studies give no evidence of chronic injury.

Toxicity in Humans

Despite these wide margins of safety in animals, dose escalation in human clinical trials with AMI-25 has shown dose-dependent acute hypotensive reactions when more than 40 μmol/kg is administered at rates greater than 1000 μmol/min [8]. So far, in the United States, 40 patients have received 20 μmol Fe/kg administered at the recommended rate of 200 μmol/min, and in only one patient was there a drop in systolic blood pressure of 20 mm Hg; no treatment was required. The mechanism of these adverse reactions is unknown. They have been reversed by infusions of saline. Further clinical trials are being conducted to explore safety and efficacy. Newer formulations with enhanced safety profiles can be anticipated also, but currently all SPIO compounds have investigational status in the United States.

Effects on MR Imaging

Numerous beneficial effects of SPIO MR contrast agents have been documented with in vivo imaging. Liver and spleen signal intensity decreases, whereas tumor nodules are displayed as areas of bright signal intensity with a variety of pulse sequences (Fig. 4) [2]. Quantitative measurements of signal-to-noise ratio (SNR) and contrast-to-noise ratio (CNR) show marked enhancement after SPIO (Table 1). Maximal decrease in signal from liver occurs on more heavily T2-weighted spin-echo (SE) pulse sequences (TR > 1000, TE > 50 msec), although relaxation effects can be shown by using a wide variety of sequences. Pulse sequences in which tumor and liver appear essentially isointense before SPIO, such as

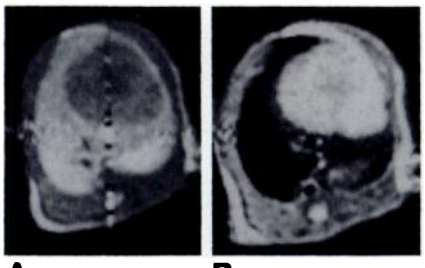

Fig. 4.—Effects of superparamagnetic iron oxide (30 μmol Fe/kg) on liver/tumor visibility in mammary carcinoma implanted in a rat.

***A*, T1-weighted MR image, SE 500/15, shows bright signal from liver outlining tumor nodule, which has slightly longer T1 relaxation time.**

***B*, MR image, SE 500/30, obtained after administration of superparamagnetic iron oxide shows complete loss of signal intensity from normal hepatic parenchyma. Tumor nodule has slightly brighter signal compared with unenhanced image because of longer TE and greater T2 weighting. Overall liver/tumor contrast is markedly increased after administration of superparamagnetic iron oxide.**

American Journal of Roentgenology 1990;155:943-950.

TABLE 1: Quantitative MR Image Analysis: Contrast- and Signal-to-Noise Ratios

Pulse Sequence	Cancer SNR	Liver SNR	Spleen SNR	Cancer-Liver CNR
Unenhanced (before drug administration)				
SE 260/14	28.7 ± 17.5	39.5 ± 12.5	27.4 ± 11.4	−10.8 ± 9.6
SE 500/28	28.1 ± 10.7	31.4 ± 9.4	26.2 ± 9.4	−3.3 ± 4.4
SE 1500/40	24.6 ± 10.9	23.9 ± 9.3	25.6 ± 13.3	+0.6 ± 4.9
SE 1500/80	19.4 ± 6.3	14.9 ± 3.9	21.3 ± 6.4	+3.4 ± 3.8
Ferrite-enhanced (1–2 hr after administration)				
SE 500/28	37.3 ± 14	21.8 ± 10.6[a]	28.5 ± 11.3	+15.9 ± 7.6[a]
SE 1500/40	24.4 ± 11.6	8.1 ± 3.7[a]	11.6 ± 4.9[a]	+16.3 ± 9.6[a]
SE 1500/80	18.9 ± 10.8	4.3 ± 3.1[a]	4.8 ± 2.3[a]	+14.5 ± 9.8[a]

Note.—Adapted from Stark et al. [8]. CNR = contrast-to-noise ratio, SNR = signal-to-noise ratio.
[a] $p < .01$; ferrite-enhanced values are significantly different from unenhanced values.

SE 500/30 (TR/TE), show great increase in tumor conspicuity after SPIO.

A further beneficial effect of increased lesion conspicuity is reduction in threshold size for lesion detection. Tsang et al. [5] conducted a detailed MR imaging/pathologic correlation of mammary tumors smaller than 1 cm implanted in rat livers. They imaged 39 separate tumor nodules 1–10 mm in diameter before and after SPIO and correlated MR appearances with thin-slice necropsy measurements. With contrast enhancement, the mean threshold size for lesion detectability decreased from 1 cm to < 3 mm in diameter. This increase in sensitivity was obtained with a 0.6-T clinical MR system by using a widely available SE 500/32 pulse sequence. These investigators further noted that even these tiny millimeter-sized nodules were not obscured on imaging or underestimated in size. Comparison of actual pathologic measurements with MR images confirmed that extremely high accuracy can be expected for clinical MR assessment of lesions. Furthermore, this study showed that enhanced CNR correlates with improved detection of lesions.

Kawamura et al. [13] confirmed these results in similar studies using a slightly larger 100-nm particle obtained from a Japanese supplier. The detection rate for 89 implanted rat tumors, including some less than 2 mm in diamter, increased from 10% (9/89) before to 65% (58/89) after ferrite injection.

The breadth of clinically advantageous SPIO effects with a variety of pulse sequence parameters was stressed in a study by Fretz et al. [14]. A range of conventional mildly T2-weighted SE sequences (500–1500/30–80) showed excellent enhancement of liver/tumor CNR at 0.6 T. Gradient-echo techniques, irrespective of TE and flip angle, showed the greatest benefit after administration of iron oxide. Gradient-echo techniques are well known to be exceptionally sensitive to the presence of local field inhomogeneities such as those produced by the presence of iron particles. Local magnetic field disturbances caused by the particles result in both irreversible (T2) and reversible dephasing of transverse coherence. Together, this transverse relaxation enhancement (T2* effect) causes extra signal loss detectable by gradient-echo techniques. The added sensitivity of gradient-echo methods may be superior to the exploitation of T2 effects with SE imaging. In our initial clinical study [8] we confirmed this effect in humans.

Clinical Results

Our group has imaged more than 40 patients with liver tumors at two sites by using mid-field systems (0.3 and 0.6 T); detailed analysis of the results in 15 of those patients has been reported [8]. Initially, doses of SPIO ranging from 10 to 50 μmol/kg were administered IV at a rate of 1 ml (11.2 mg Fe)/min in a dose-escalation study. On the basis of toxicity data, the recommended clinical dose for AMI-25 has been set at 10–20 μmol Fe/kg body weight. The ultimate dose of SPIO that will be allowed by the Food and Drug Administration (if approved) has yet to be established. Imaging usually has been performed within 1 hr after injection, although satisfactory clinical imaging results easily could be achieved as late as 48 hr.

Profound reduction in both liver and spleen signal intensity was seen in all patients, even as early as 5 min after SPIO administration (Fig. 5). As expected, cancer tissue was unaffected, and striking improvements in the sensitivity of lesion detection occurred when compared with unenhanced images (Fig. 6). The beneficial effect on lesion detection occurred with a range of conventional pulse sequences. Overall, the number of lesions detected after contrast administration increased from 89 to 349 on SE 500/28 images, from 21 to 325 on SE 1500/40 images, and from 20 to 271 on SE 1500/80 images (of a total of 370 lesions identified). Quantitative analyses of lesion/liver CNR values confirm the subjective visual appearances, as shown in Table 1.

In patients with known hepatic metastases, lesions smaller than 1 cm in diameter were not visible on unenhanced SE images with TRs of 500 and 1500 msec, whereas threshold size for lesion detection on unenhanced SE 260/14 images was 0.5 cm when a 0.6-T MR imaging system was used. After administration of contrast material, many lesions 0.3–1.0 cm could be detected (Fig. 7). The size threshold for lesion detectability decreased from 1.5 to 0.3 cm on SE 500/28 images, from 2.1 to 0.3 cm on SE 1500/40 images, and from 1.9 to 0.4 cm on SE 1500/80 images. These results were statistically significant at $p < .005$.

In order to provide more objective documentation of the benefits of SPIO for detection of liver cancer, quantitative comparisons of diagnostic accuracy were made by using receiver-operating-characteristic (ROC) analysis. Fretz et al.

American Journal of Roentgenology 1990;155:943-950.

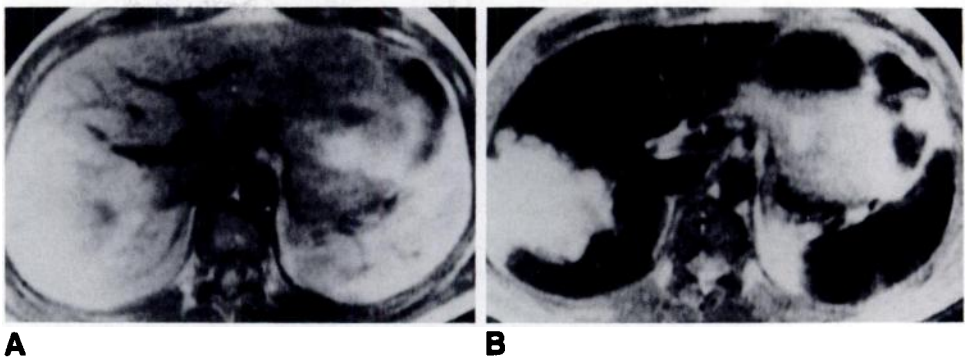

Fig. 5.—Metastatic colonic cancer.
***A*, Unenhanced SE 1500/40 MR image shows a mass displacing vessels in posterior segment of right hepatic lobe. Contrast between tumor and liver is low and exact margins of tumor are difficult to delineate.**
***B*, 1 hr after IV administration of superparamagnetic iron oxide (AMI-25, 40 μmol Fe/kg). Tumor is now easily detected, sharply delineated, and distinguished from adjacent blackened liver tissue. Note corresponding signal decrement in the spleen.**
(Reprinted from Weissleder et al. [15].)

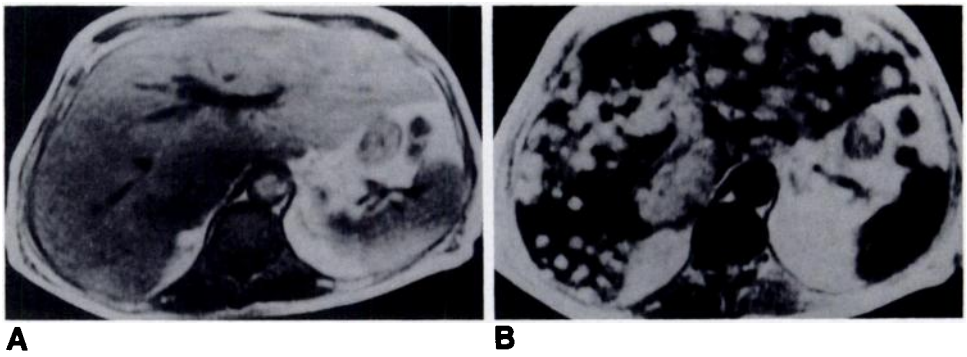

Fig. 6.—Improvement in sensitivity for lesion detection in patient with metastatic renal cell carcinoma.
***A*, T1-weighted SE 500/28 MR image before ferrite administration shows normal upper abdominal anatomy. Poorly defined region of low intensity is seen near caudate lobe of liver.**
***B*, Same sequence at same anatomic level 15 min after administration of AMI-25 (20 μmol/kg). Diffuse hepatic metastases, many smaller than 0.5 cm in diameter, can be identified. Large lesion in region of caudate lobe corresponds to area of abnormal signal on unenhanced image. Note reduction in signal of spleen.**
(Reprinted with permission from Stark et al. [8].)

American Journal of Roentgenology 1990.155:943-950.

[17] performed a controlled observer-performance test of contrast-enhanced CT, unenhanced MR, and MR after AMI-25 on 731 individual images from our clinical trial material. Contrast-enhanced MR yielded significantly better observer-performance scores than did bolus contrast-enhanced CT images, whereas enhanced SE 1500/40 and 1500/80 sequences yielded significantly greater areas under the ROC curve than did standard MR sequences. The superiority of SPIO-enhanced MR over iodine-enhanced CT and unenhanced MR imaging was statistically significant ($p < .01$) in both cases.

In a study of 15 patients in whom liver metastases were imaged at high field (1.5 T), Marchal et al. [9] found comparable quantitative gains in CNR on all sequences except heavily T2-weighted SE (2200/70) [9]. With this sequence there was only marginal benefit after SPIO administration. The optimal relation between imager field strength, pulse sequence, and SPIO needs to be clarified in future clinical studies.

Enhanced Spleen Imaging

None of the currently available techniques, including CT scanning, are very sensitive to either metastatic disease or lymphomatous involvement of the spleen. Detection of splenic deposits by MR also has been unreliable because of the similarity of spleen relaxation times (T1 and T2) and proton density to the MR characteristics of tumor tissue. As a result, there is little net difference in the tumor-spleen signal intensity on most pulse sequences. However, as in the case of hepatic metastases, SPIO selectively alters the tissue characteristics (T2) of spleen without affecting tumor, producing a marked increase in image contrast and detectability of splenic tumor deposits.

Early studies by Weissleder et al. [4] from our group showed that 4- to 6-mm splenic tumors implanted in animal models become readily visible after SPIO administration (Fig. 8). Tumors appear hyperintense against the black background of spleen tissue because, again, the SPIO is not sequestered by tumor tissue. Quantitative measurements of lesion conspicuity measured by tumor-spleen CNR ratios also showed 40- to 50-fold increases. In a subsequent series of 18 patients, SPIO-enhanced MR revealed 45 individual splenic nodules (four patients were positive) as opposed to four lesions on unenhanced images (two patients were positive) (Fig. 9) [16]. Because the effect of SPIO is less in splenic pulp than in liver, the dose of iron necessary to achieve comparable degrees of spleen blackening may be slightly larger (i.e., 20–30 μmol Fe/kg body weight).

Of perhaps even greater clinical significance is the ability of SPIO to reveal diffuse lymphomatous involvement of the spleen. In lymphoma patients, splenomegaly per se is an unreliable indicator of active neoplastic infiltrate. Our group developed techniques for SPIO-enhanced MR to detect both micronodular lymphoma and diffuse lymphoma in animal models [7]. Moreover, benign splenomegaly was differentiated by its preservation of complete blackening after SPIO, whereas spleens with diffuse malignant lymphoma showed no iron uptake. Lymphomatous spleens retained their diffuse bright signal after SPIO, presumably because RES phagocytic

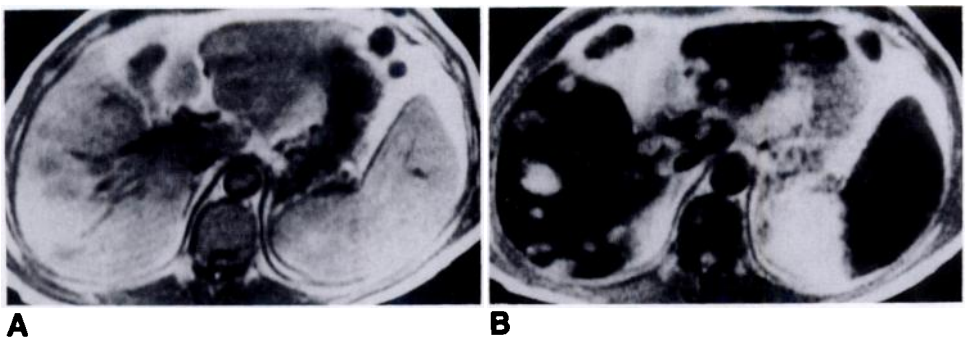

Fig. 7.—Demonstration of hepatic and splenic metastases after AMI-25 administration.

A, Unenhanced T1-weighted SE 500/28 MR image. Several 1- to 3-cm metastases are visible in right hepatic lobe. Questionable area of reduced signal intensity in medial portion of spleen was thought to be an artifact.

B, Mildly T2-weighted SE 1500/42 sequence 1 hr after injection of contrast material. Multiple additional small hepatic lesions measuring 5–10 mm are evident in both right and left hepatic lobes. In addition, entire medial portion of spleen is replaced by large solitary metastatic deposit. Splenic tumor was confirmed at splenectomy.

(Reprinted with permission from Weissleder et al. [16].)

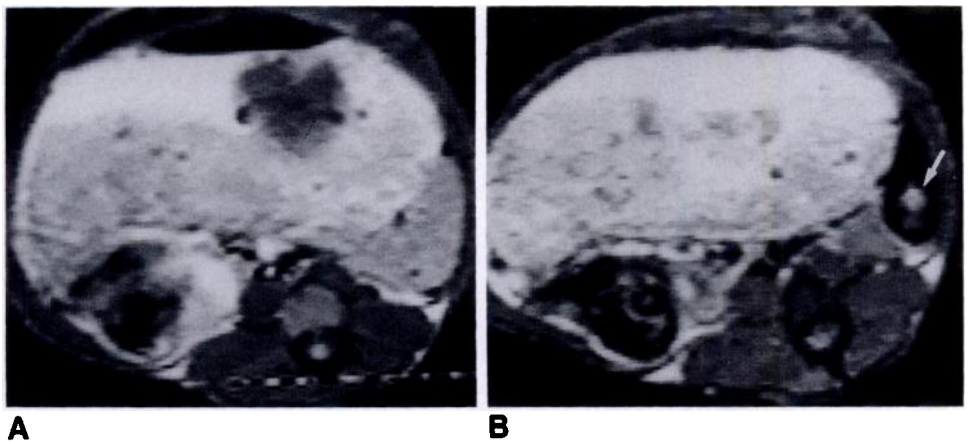

Fig. 8.—Demonstration of splenic tumor in animal model after administration of superparamagnetic iron oxide (SPIO).

A, SE 500/32 MR image before SPIO shows no abnormality within spleen.

B, After administration of SPIO, blackening of spleen parenchyma shows tumor nodule because of markedly enhanced tumor/spleen contrast (*arrow*).

activity was blocked by malignant infiltrate. In patients with normal spleens and in those with benign splenomegaly, spleen signal intensity showed the typical marked blackening after ferrite. These findings were confirmed in four subjects in a preliminary clinical investigation [15].

The results suggest that both metastatic and lymphomatous neoplasms of the spleen, whether focal or diffuse, may be diagnosed with improved accuracy with SPIO-enhanced MR images.

Cirrhosis and Hepatitis

Striking morphologic and functional effects were seen after SPIO administration in a small pilot series of seven patients with cirrhosis and active alcoholic hepatitis [18]. Cirrhotic liver tissue showed an inhomogeneous decrease in liver signal intensity with a superimposed reticular nodular pattern of thin septa of high signal intensity believed to represent collagenous bands. Splenomegaly with marked signal loss confirmed the well-known redistribution of particulate matter occurring in cirrhotic portal hypertension. Patients with active hepatitis showed a markedly reduced hepatic response to iron oxide, with effective preservation of normal signal intensity. This effect was thought to reflect diminished Kupffer cell activity. The results were considered highly promising as a means to further characterize diffuse liver disease.

Image Interpretation

As with any fundamentally new imaging technique, SPIO-enhanced MR imaging raises complex interpretative issues for the radiologist.

Because the liver turns dark on all pulse sequences, tumor nodules are always higher in signal intensity than surrounding liver. However, signal in blood vessels viewed in cross section may resemble millimeter-sized tumors. To overcome this pitfall, Hahn et al. [19] performed imaging during the first 12 min after ferrite injection while the contrast agent remains in circulation (distribution phase). They showed reduction of signal from small intrahepatic blood vessels, as the entire liver became uniformly blackened, allowing greater confidence in distinguishing tumor from vessels in cross section. Distribution-phase images showed little or no signal loss from cancer tissue. Vascular signal was restored on images at 1–2 hr (retention phase).

A further major problem in clinical cancer imaging is differentiation of malignant nodules from incidental coexisting benign tumors, especially the common cavernous hemangioma. In the same study, Hahn et al. [19] found that hemangiomas showed greater signal loss on retention-phase images (1–2 hr after injection) than did metastatic lesions (Fig. 10). Intralesional signal intensity loss of 60% or more of the unenhanced intensity was characteristic of cavernous hemangioma. These findings confirm the slower and prolonged perfusion of cav-

American Journal of Roentgenology 1990;155:943-950.

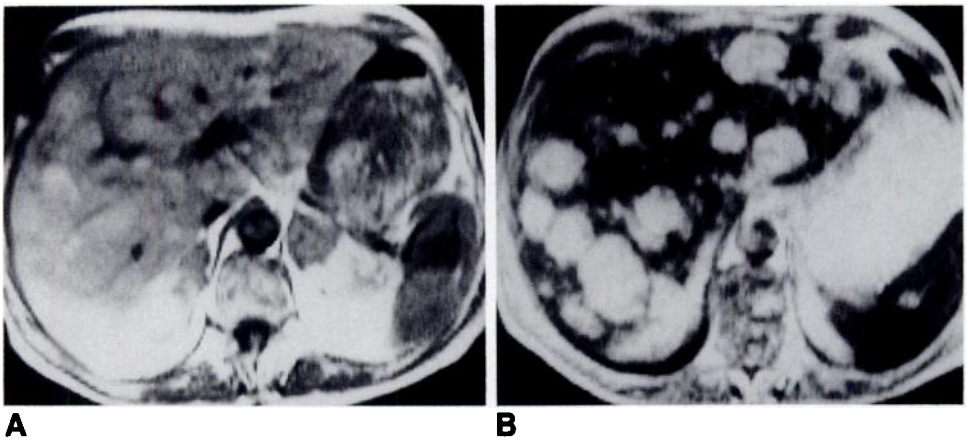

Fig. 9.—Enhanced detection of splenic tumor nodules in a patient with widespread hepatic metastases.

***A*, SE 1500/40 MR image faintly shows several bright-signal liver metastases. No definite abnormality is evident in spleen.**

***B*, After AMI-25 administration, a single discrete tumor nodule is visible in spleen. Liver metastases are more visible, with numerous small subcentimeter nodules now evident.**

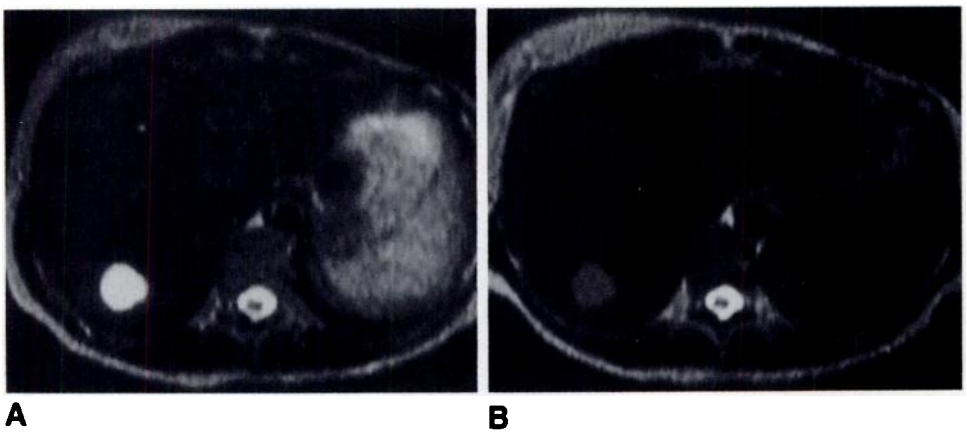

Fig. 10.—Cavernous hemangioma showing negative contrast enhancement after AMI-25 administration. The lesion was considered atypical because of poor contrast enhancement on CT.

***A* and *B*, Heavily T2-weighted SE 2350/180 MR images before (*A*) and 2 hr after (*B*) injection of AMI-25 (20 μmol Fe/kg). Hemangioma loses signal because of retention of agent in vascular pool of lesion. (Reprinted with permission from Hahn et al. [19].)**

ernous hemangiomas observed with other imaging studies. Although SPIO perfusion effects hold great promise for providing tissue characterization, more studies are required for confirmation. Similar strategies are used to diagnose hemangiomas by blood-pool imaging of iodine (CT), ^{99m}Tc-labeled erythrocytes (nuclear medicine), or gadopentetate dimeglumine–enhanced MR.

In the context of tissue characterization by MR, there are two further caveats. First, the use of signal-intensity measurements or calculated T2 relaxation times may give spurious results when lesion/liver ratios are applied to patients in whom liver T2 is shortened by iron [20]. Specifically, the presence of exogenously administered iron oxide variably alters both hemangioma and liver signal intensities, eliminating the very long T2 of hemangiomas while changing (unpredictably) their signal-intensity ratio relative to liver.

Second, certain primary liver tumors or tumorlike conditions, such as hepatic adenoma and focal nodular hyperplasia, may contain Kupffer cells. SPIO may cause such lesions to lose signal, even in the retention phase. This would tend to obscure the lesion but might have value in suggesting a tissue-specific diagnosis.

Conclusions

The value of SPIO-enhanced MR imaging of the liver and spleen has been accepted rapidly by the medical research community. Further clinical experience must be accumulated to validate its clinical role. A first priority will be to establish a clear safety profile for the various formulations under development. New commercial formulations may extend the safety margins. Biodistribution, clearance, and protocols for clinical administration may or may not be altered for various SPIOs.

Future research directions will involve the use of SPIO for splenic neoplasia, especially lymphomas; diffuse liver diseases; bone marrow and lymph node imaging; and perfusion studies. Cardiac studies in which SPIO is combined with high-speed gradient-echo or echo planar imaging techniques offer an especially interesting possibility. The ability of these methods to permit further reduction of the SPIO dose certainly will be studied extensively in clinical trials. Finally, in the liver, where the first clinical applications are likely, more detailed definition of cellular function and temporal profiles of SPIO retention within benign and malignant liver tumors will be necessary to refine diagnostic criteria for clinical use. The agent appears to have a promising future in clinical MR imaging.

REFERENCES

1. Saini S, Stark DD, Hahn PF, Wittenberg J, Brady TJ, Ferrucci JT Jr. Ferrite particles: a superparamagnetic MR contrast agent for the reticuloendothelial system. *Radiology* **1987**;162:211–216

American Journal of Roentgenology 1990;155:943-950.

2. Saini S, Stark DD, Hahn PF, et al. Ferrite particles: a superparamagnetic MR contrast agent for enhanced detection of liver carcinoma. *Radiology* **1987**;162:217–222
3. Bacon BR, Stark DD, Park CH, et al. Ferrite particles: a new magnetic resonance imaging contrast agent: lack of acute or chronic hepatotoxicity after intravenous administration. *J Lab Clin Med* **1987**;110(2):164–171
4. Weissleder R, Hahn PF, Stark DD, et al. MR imaging of splenic metastases: ferrite-enhanced detection in rats. *AJR* **1987**;149:723–726
5. Tsang YM, Stark DD, Chen MCM, Weissleder R, Wittenberg J, Ferrucci JT. Hepatic micrometastases in the rat: ferrite-enhanced MR imaging. *Radiology* **1988**;167:21–24
6. Weissleder R, Stark DD, Engelstad BL, et al. Superparamagnetic iron oxide: pharmacokinetics and toxicity. *AJR* **1989**;152:167–173
7. Weissleder R, Stark DD, Rummeny EJ, Compton CC, Ferrucci JT. Splenic lymphoma: ferrite-enhanced MR imaging in rats. *Radiology* **1988**;166: 423–430
8. Stark DD, Weissleder R, Elizondo G, et al. Superparamagnetic iron oxide: clinical application as a contrast agent for MR imaging of the liver. *Radiology* **1988**;168:297–301
9. Marchal G, Van Hecke P, Demaerel P, et al. Detection of liver metastases with superparamagnetic iron oxide in 15 patients: results of MR imaging at 1.5 T. *AJR* **1989**;152:771–775
10. Blakemore RP, Frankel R. Magnetic navigation in bacteria. *Sci Am* **1981**;246:58–65
11. Bean CP. Hysteresis loops of mixtures of ferromagnetic micropowders. *J Appl Phys* **1955**;26:1381–1383
12. Patrizio G, Elizondo G, Fretz C, Eley CGS, Stark DD, Ferrucci JT. Cancer targeted liposomes containing superparamagnetic iron oxide: ferrosomes (abstr.). In: *Book of abstracts. Society of Magnetic Resonance in Medicine. Eighth annual meeting,* vol. 1. Berkeley, CA: Society of Magnetic Resonance in Medicine, **1989**:327
13. Kawamura Y, Endo Y, Watanabe Y, et al. Use of magnetite particles as a contrast agent for MR imaging of the liver. *Radiology* **1990**;174:357–360
14. Fretz CJ, Elizondo G, Weissleder R, Hahn PF, Stark DD, Ferrucci JT Jr. Superparamagnetic iron oxide-enhanced MR imaging: pulse sequence optimization for detection of liver cancer. *Radiology* **1989**;172:393–397
15. Weissleder R, Elizondo G, Stark DD, et al. The diagnosis of splenic lymphoma by MR imaging: value of superparamagnetic iron oxide. *AJR* **1989**;152:175–180
16. Weissleder R, Hahn PF, Stark DD, et al. Superparamagnetic iron oxide: enhanced detection of focal splenic tumors with MR imaging. *Radiology* **1988**;169:399–403
17. Fretz CJ, Stark DD, Metz CE, et al. Detection of hepatic metastases: comparison of contrast-enhanced CT, unenhanced MR imaging, and iron oxide-enhanced MR imaging. *AJR* **1990**;155:763–770
18. Elizondo G, Weissleder R, Stark DD, et al. Hepatic cirrhosis and hepatitis: MR imaging enhanced with superparamagnetic iron oxide. *Radiology* **1990**;174:797–801
19. Hahn PF, Stark DD, Weissleder R, Elizondo G, Saini S, Ferrucci JT. Clinical application of superparamagnetic iron oxide to MR imaging of tissue perfusion vascular liver tumors. *Radiology* **1990**;174:361–366
20. Mirowitz S, Heiken JP, Lee JKT. Potential MR pitfall in relying on lesion/liver ratio in presence of hepatic hemochromatosis. *J Comput Assist Tomogr* **1988**;12:323–324

American Journal of Roentgenology 1990.155:943-950.